2013

Block copolymer/ferroelectric nanoparticle nanocomposites

Xinchang Pang
Georgia Institute of Technology - Main Campus

Yanjie He
Georgia Institute of Technology - Main Campus

Beibei Jiang
Georgia Institute of Technology - Main Campus

James Iocozzia
Georgia Institute of Technology - Main Campus

Lei Zhao
Georgia Institute of Technology - Main Campus

See next page for additional authors

Block copolymer/ferroelectric nanoparticle nanocomposites

Abstract
Nanocomposites composed of diblock copolymer/ferroelectric nanoparticles were formed by selectively constraining ferroelectric nanoparticles (NPs) within diblock copolymer nanodomains via judicious surface modification of ferroelectric NPs. Ferroelectric barium titanate ($BaTiO_3$) NPs with different sizes that are permanently capped with polystyrene chains (i.e., PS-functionalized $BaTiO_3$NPs) were first synthesized by exploiting amphiphilic unimolecular star-like poly(acrylic acid)-block-polystyrene (PAA-b- PS) diblock copolymers as nanoreactors. Subsequently, PS-functionalized $BaTiO_3$ NPs were preferentially sequestered within PS nanocylinders in the linear cylinder-forming polystyrene-block-poly(methyl methacrylate) (PS-b-PMMA) diblock copolymer upon mixing the $BaTiO_3$ NPs with PS-b-PMMA. The use of PS-b-PMMA diblock copolymers, rather than traditional homopolymers, offers the opportunity for controlling the spatial organization of PS-functionalized $BaTiO_3$ NPs in the PS-b-PMMA/$BaTiO_3$ NP nanocomposites. Selective solvent vapor annealing was utilized to control the nanodomain orientation in the nanocomposites. Vertically oriented PS nanocylinders containing PS-functionalized $BaTiO_3$ NPs were yielded after exposing the PS-b-PMMA/$BaTiO_3$ NP nanocomposite thin film to acetone vapor, which is a selective solvent for PMMA block. The dielectric properties of nanocomposites in the microwave frequency range were investigated. The molecular weight of PS-b-PMMA and the size of $BaTiO_3$ NPs were found to exert an apparent influence on the dielectric properties of the resulting nanocomposites.

Disciplines
Chemistry | Materials Science and Engineering | Polymer and Organic Materials

Comments
This article is from *Nanoscale*5 (2013): 8695-8702, doi: 10.1039/c3nr03036a. Posted with permission.

Authors
Xinchang Pang, Yanjie He, Beibei Jiang, James Iocozzia, Lei Zhao, Hanzheng Guo, Jin Liu, Mufit Akinc, Nicola Bowler, Xiaoli Tan, and Zhiqun Lin

Nanoscale

RSC Publishing

PAPER

View Article Online
View Journal | View Issue

Block copolymer/ferroelectric nanoparticle nanocomposites†

Cite this: *Nanoscale*, 2013, **5**, 8695

Xinchang Pang,[a] Yanjie He,[a] Beibei Jiang,[a] James Iocozzia,[a] Lei Zhao,[a] Hanzheng Guo,[b] Jin Liu,[b] Mufit Akinc,[b] Nicola Bowler,[b] Xiaoli Tan[b] and Zhiqun Lin*[a]

Nanocomposites composed of diblock copolymer/ferroelectric nanoparticles were formed by selectively constraining ferroelectric nanoparticles (NPs) within diblock copolymer nanodomains *via* judicious surface modification of ferroelectric NPs. Ferroelectric barium titanate ($BaTiO_3$) NPs with different sizes that are permanently capped with polystyrene chains (*i.e.*, PS-functionalized $BaTiO_3$NPs) were first synthesized by exploiting amphiphilic unimolecular star-like poly(acrylic acid)-*block*-polystyrene (PAA-*b*-PS) diblock copolymers as nanoreactors. Subsequently, PS-functionalized $BaTiO_3$ NPs were preferentially sequestered within PS nanocylinders in the linear cylinder-forming polystyrene-*block*-poly(methyl methacrylate) (PS-*b*-PMMA) diblock copolymer upon mixing the $BaTiO_3$ NPs with PS-*b*-PMMA. The use of PS-*b*-PMMA diblock copolymers, rather than traditional homopolymers, offers the opportunity for controlling the spatial organization of PS-functionalized $BaTiO_3$ NPs in the PS-*b*-PMMA/$BaTiO_3$ NP nanocomposites. Selective solvent vapor annealing was utilized to control the nanodomain orientation in the nanocomposites. Vertically oriented PS nanocylinders containing PS-functionalized $BaTiO_3$ NPs were yielded after exposing the PS-*b*-PMMA/$BaTiO_3$ NP nanocomposite thin film to acetone vapor, which is a selective solvent for PMMA block. The dielectric properties of nanocomposites in the microwave frequency range were investigated. The molecular weight of PS-*b*-PMMA and the size of $BaTiO_3$ NPs were found to exert an apparent influence on the dielectric properties of the resulting nanocomposites.

Received 13th June 2013
Accepted 5th July 2013

DOI: 10.1039/c3nr03036a

www.rsc.org/nanoscale

Introduction

Nanocomposite materials offer a vast design space of potential material properties, depending on the properties of the constituents and their spatial arrangement.[1] Nanocomposites of a polymer and nanoparticles (NPs) yielded by incorporating NPs into a polymer matrix often exhibit advantageous optical, electrical, and mechanical performance enhancement when compared to non-hybrid counterparts.[1] The spatial control of NPs in different polymeric domains is of great interest for practical applications such as nanostructured solar cells,[2] high efficiency catalysts, photonic band-gap materials,[3,4] high-density magnetic storage media,[5] microwave devices,[6,7] sensors,[8] capacitors,[9] and so on.[1] In this regard, block copolymers (BCPs) composed of chemically dissimilar chains offer the possibility to precisely control the NP organization at the nanoscale.[10,11]

Two major approaches have been developed for incorporating inorganic NPs into BCPs to form BCP-based nanocomposites. The first approach involves the *in situ* synthesis of NPs within a BCP domain containing the NP precursors.[12] In contrast, the second approach uses the cooperative self-organization of preformed NPs and BCPs,[12] where the location of NPs within the BCP can be controlled by exploiting the enthalpic interaction between the BCP and the surface-modified (*e.g.*, polymer-coated) NPs.[11] The polymeric ligands on the NP surface control and stabilize the NP formation, allowing the initial small size to be retained by preventing NPs from aggregation. Meanwhile, by specifying the chemical nature of these polymeric ligands so they interact more favorably with one block in the BCP (*i.e.*, preferential segregation within the target block), they provide an ability to control the placement of NPs within the BCP.[11,13] However, this strategy requires the synthesis of polymeric ligands that are chemically identical or similar to one of the blocks in the BCP for the surface functionalization of NPs.[12]

Barium titanate ($BaTiO_3$) is one of the most extensively studied ferroelectric materials due to its high dielectric constant and ferroelectric properties at temperature below 130 °C where it assumes a ferroelectric phase.[14] It finds use in a variety of areas that include multilayer capacitors, transducers,

[a]*School of Materials Science and Engineering, Georgia Institute of Technology, Atlanta, GA 30332, USA. E-mail: zhiqun.lin@mse.gatech.edu*

[b]*Department of Materials Science and Engineering, Iowa State University, Ames, Iowa 50011, USA*

† Electronic supplementary information (ESI) available: Summary of data for star-like PAA-*b*-PS, ^{1}H-NMR, XRD, EDS, TGA, TEM and AFM images. See DOI: 10.1039/c3nr03036a

actuators, and electro-optical devices.[15,16] The ferroelectric and dielectric properties of $BaTiO_3$ depend heavily on its size and density.[17,18] Conventionally, $BaTiO_3$ is prepared by heating a mixture of $BaCO_3$ and TiO_2 at a temperature above 1300 °C.[14] This procedure leads to powders that are coarse and inhomogeneous in size. Another problem concerned with this synthesis is the high cost required due to high-temperature sintering.[15] Novel strategies that allow for the preparation of homogeneous $BaTiO_3$ at relatively low temperature are highly desirable to obtain fine particles for myriad applications.[16,19] Soft-chemical processes such as the hydrothermal method,[20,21] the sol–gel process,[22,23] and the precursor decomposition method[24,25] have been intensively used to prepare $BaTiO_3$ NPs.[16] These approaches carry advantages over the conventional solid state reactions as the nucleation in aqueous solution and subsequent crystalline growth proceed at much lower temperature.[16]

Herein, we report the formation of nanostructured composites based on block copolymers, incorporating ferroelectric nanoparticles within the target block of the copolymer. Polystyrene-capped $BaTiO_3$ nanoparticles (PS-functionalized $BaTiO_3$ NPs) with different average sizes were first synthesized by utilizing a new class of amphiphilic unimolecular star-like poly(acrylic acid)-*block*-polystyrene (PAA-*b*-PS) diblock copolymers, prepared by sequential atom transfer radical polymerization (ATRP), as nanoreactors. As the surface of $BaTiO_3$ NPs was permanently capped with PS chains, it dispensed with the need for further surface modification of NPs as in copious past work. Subsequently, hybrid nanomaterials composed of linear cylinder-forming polystyrene-*block*-poly(methyl methacrylate) (PS-*b*-PMMA) diblock copolymers and PS-functionalized $BaTiO_3$ NPs were yielded upon mixing. The $BaTiO_3$ NPs were selectively dispersed in the cylindrical PS nanodomains of PS-*b*-PMMA due to the selective chemical affinity of PS-functionalized $BaTiO_3$ NPs to the PS block against aggregation, *i.e.*, possessing a neutral $\chi_{NP-Polymer}$, where $\chi_{NP-Polymer}$ represents the chemical affinity of the NP to the PS block (*i.e.*, enthalpic interaction). By exposing a thin film of PS-*b*-PMMA–PS-capped $BaTiO_3$ NP nanocomposites to acetone vapor, which is a selective solvent for PMMA, vertically oriented PS nanocylinders containing $BaTiO_3$ NPs were achieved. Finally, the dielectric properties of nanocomposites as a function of microwave frequency from 2 GHz to 15 GHz were explored, revealing that the dielectric properties of these ferroelectric nanocomposites are dependent on the molecular weight of PS-*b*-PMMA and the size of $BaTiO_3$ NPs.

Experimental section

Materials

Two asymmetric linear PS-*b*-PMMA diblock copolymers (M_{PS} = 45 900 g mol^{-1} and M_{PMMA} = 138 000 g mol^{-1} with polydispersity, PDI = 1.10; M_{PS} = 315 000 g mol^{-1} and M_{PMMA} = 785 000 g mol^{-1} with PDI = 1.20) were purchased from Polymer Source Inc. Three amphiphilic 21-arm, star-like poly(acrylic acid)-*block*-polystyrene (PAA-*b*-PS) diblock copolymers with different molecular weights were synthesized according to our previous work.[26] *N*,*N*-Dimethylformamide (DMF, Fisher Scientific, 99.9%) was distilled over CaH_2 under reduced pressure prior to use. Barium chloride dihydrate ($BaCl_2 \cdot 2H_2O$, ≥99.0%), titanium(IV) chloride ($TiCl_4$, ≥99.0%) and sodium hydroxide (NaOH, ≥98%) were purchased from Sigma-Aldrich, and used as received.

Synthesis of $BaTiO_3$ NPs with different sizes

Three amphiphilic 21-arm, star-like PAA-*b*-PS diblock copolymers (Table S1†) with tailorable architectures, different molecular weights, and different ratios of PAA to PS blocks were then used as nanoreactors to produce $BaTiO_3$ NPs capped with PS chains. Ferroelectric $BaTiO_3$ NPs were synthesized *via* a wet chemistry approach by reacting NP precursors with the inner PAA chains of star-like PAA-*b*-PS diblock copolymers. In a typical process, 10 mg star-like PAA-*b*-PS (sample-2 in Table S1†) template was dissolved in 10 mL DMF at room temperature, followed by the addition of an appropriate amount of precursors (*i.e.*, $BaCl_2 \cdot 2H_2O$ + $TiCl_4$ + NaOH; 0.081 g + 0.0658 g + 0.0139 g) that were selectively incorporated into the space occupied by the inner PAA blocks through the coordination bonding between the carboxyl of PAA and the metal ions of precursors as there were no active functional groups in the outer PS blocks to coordinate with the precursors. The solution was then refluxed at 180 °C under Ar for 2 h, yielding ferroelectric $BaTiO_3$ NPs (sample-b; diameter, D = ~11 nm) capped with PS. $BaTiO_3$ NPs of different diameters capped with PS (*i.e.*, sample-a, D = ~6 nm; sample-c, D = ~27 nm) were also prepared using the same approach with star-like PAA-*b*-PS of different molecular weights as templates (*i.e.*, sample 1 and sample 3 in Table S1,† respectively).

Sample preparation

Two linear PS-*b*-PMMA diblock copolymers (*i.e.*, M_{PS} = 45 900 and M_{PMMA} = 138 000; M_{PS} = 315 000 and M_{PMMA} = 785 000) were dissolved in toluene, forming 5 mg mL^{-1} solutions. To prepare nanocomposite samples, PS-functionalized $BaTiO_3$ NP powder was added into 5 mg mL^{-1} PS-*b*-PMMA diblock copolymer toluene solution to produce a series of nanocomposites with different weight fractions of $BaTiO_3$ NPs. Thin films of nanocomposites of PS-*b*-PMMA–PS-functionalized $BaTiO_3$ NPs were formed on freshly cleaned Si wafers by spin-coating the toluene solution at 3000 rpm for 40 s. These thin films were then immediately placed in an airtight 30 cm^3 glass vessel containing 50 μL acetone for a certain period of time at room temperature (*i.e.*, a solvent vapor annealing process). After being exposed to the acetone vapor for a certain period of time, the samples were then quickly removed from the vessel and dried in air at room temperature.

Characterization

The size and morphology of PS-functionalized $BaTiO_3$ NPs, and morphology of thin films of PS-*b*-PMMA/$BaTiO_3$ NP nanocomposites were examined by transmission electron microscopy (TEM) (JEOL 1200EX scanning/transmission electron microscope (STEM); operated at 80 kV). The PS-functionalized $BaTiO_3$ NPs were dissolved in toluene at a very low

concentration. TEM samples of PS-functionalized $BaTiO_3$ NPs were prepared by applying a drop of $BaTiO_3$ NP toluene solution onto a carbon-coated copper TEM grid (300 mesh) and allowing toluene to evaporate under ambient conditions. The morphology of the nanocomposite films after acetone vapor annealing was also characterized by TEM. To prepare the nanocomposite TEM sample, the nanocomposite thin film formed on the Si substrate coated with 200 nm thick SiO_2 on its surface was immersed into dilute hydrofluoric acid (HF) aqueous solution; the film was then spontaneously delaminated from the Si surface and floated on the top of water. Subsequently, a TEM grid was placed in contact with the floating film, thereby transferring the film onto the surface of the TEM grid. Finally, the grid was exposed to ruthenium tetraoxide (RuO_4), with which the PS phase was preferentially stained. As a result, PS nanodomains appeared dark in the TEM images. Energy dispersive X-ray spectroscopy (EDS) analysis of nanocomposites was performed using a field-emission scanning electron microscope (FESEM; FEI Quanta250 operating at 10 kV in high vacuum). The crystalline structures of the nanocomposites were measured by X-ray diffraction (XRD; SCINTAGXDS-2000, Cu Kα radiation ($\lambda = 0.154$ nm)). The weight fraction of the polymer phase in the nanocomposites was determined by thermogravimetric analysis (TGA; TA Instrument TGA Q 50). The thickness of the films was measured by Atomic Force Microscopy (AFM; Dimension 3000). To characterize the dielectric properties of nanocomposites in the microwave frequency range, two pure PS-*b*-PMMA diblock copolymers ($M_{PS} = 45\,900$ and $M_{PMMA} = 138\,000$; $M_{PS} = 315\,000$ and $M_{PMMA} = 785\,000$) and their corresponding nanocomposites containing approximately 10–11% (by volume) of PS-functionalized $BaTiO_3$ NPs of different sizes (*i.e.*, $D = \sim 11$ nm, denoted PS-BTO11 (sample-b), and $D = \sim 27$ nm, PS-BTO27 (sample-c)) were hot-pressed into a toroidal shape (with rectangular surface of revolution) with inner and outer diameters of 3.00 ± 0.05 mm and 7.00 ± 0.05 mm, respectively, and thickness in the range from 0.5–1.0 mm. The complex permittivity of the nanocomposites was measured with a Vector Network Analyzer (Anritsu 37347C) incorporating a *S*-parameter test set and operating in the 2–15 GHz microwave frequency region. The *S*-parameters were determined by using the coaxial transmission/reflection method and converted to complex permittivity by application of the Nicholson–Ross–Weir algorithm.[27,28]

Results and discussion

In contrast to traditional approaches such as high-temperature sintering,[15] or the soft-chemical approach,[16,29,30] $BaTiO_3$ NPs with tunable sizes were prepared by exploiting a series of star-like PAA-*b*-PS diblock copolymers as nanoreactors. The star-like PAA-*b*-PS was composed of inner hydrophilic PAA blocks and outer hydrophobic PS blocks with each arm covalently linked to a small molecule β-cyclodextrin (β-CD).[31] Three star-like PAA-*b*-PS diblock copolymers with different molecular weights and ratios of PAA to PS blocks were synthesized by sequential atom transfer radical polymerization (ATRP),[26,32] in which β-CD-based star-like 21-Br-β-CD with 21 initiating sites was used as a macroinitiator (Scheme S1†).[26] These star-like diblock copolymers with well-controlled molecular architectures and molecular weights form structurally stable spherical *unimolecular* micelles. The inner PAA block in the micelles is highly hydrophilic and facilitates the preferential incorporation of $BaTiO_3$ precursors in the space occupied by PAA blocks *via* a strong coordination bonding between the metal ion of precursors and functional groups of PAA (*i.e.*, carboxyl). Notably, there was no such coordination with the outer PS chains. Subsequent hydrolysis and condensation of precursors in pure DMF yielded $BaTiO_3$ NPs, in which the surface of NPs was permanently connected with PS chains (*i.e.*, PS-functionalized $BaTiO_3$ NPs), rendering the solubility of PS-functionalized $BaTiO_3$ NPs in organic solvents (Scheme 1A).

The diameter of $BaTiO_3$ NPs can be readily altered by varying the chain length of the PAA block during ATRP of *tert*-butyl acrylate (*i.e.*, forming poly(*tert*-butyl acrylate) (P*t*BA)), which was subsequently hydrolyzed into PAA (Scheme S1†). Three $BaTiO_3$ NPs with diameters of $D = 6.3 \pm 1.3$ nm, 11.2 ± 1.9 nm, and 27.1 ± 3.1 nm (Fig. 1) were obtained by utilizing three different star-like PAA-*b*-PS as nanoreactors with molecular weights of PAA blocks, $M_{PAA} = 4500$, $M_{PAA} = 8400$, and $M_{PAA} = 28\,100$, respectively (Table S1†). The representative high resolution TEM (HRTEM) characterization revealed that these $BaTiO_3$ NPs possessed a continuous crystalline lattice. It is noteworthy that the presence of intimately connected hydrophobic PS chains on the surface of $BaTiO_3$ NPs is crucial as they promote the

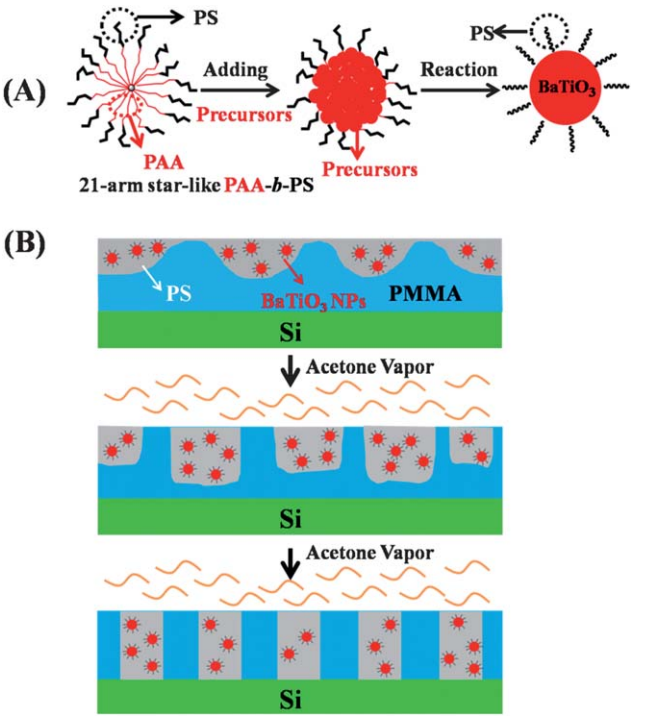

Scheme 1 (A) Synthesis of $BaTiO_3$ NPs permanently capped with PS chains by using amphiphilic star-like PAA-*b*-PS diblock copolymers as nanoreactors. (B) Schematic representation of the formation of vertically oriented PS nanocylinders containing $BaTiO_3$ NPs upon selective solvent acetone vapor annealing of PS-*b*-PMMA–PS-functionalized $BaTiO_3$ NP nanocomposites spin-coated on the Si substrate.

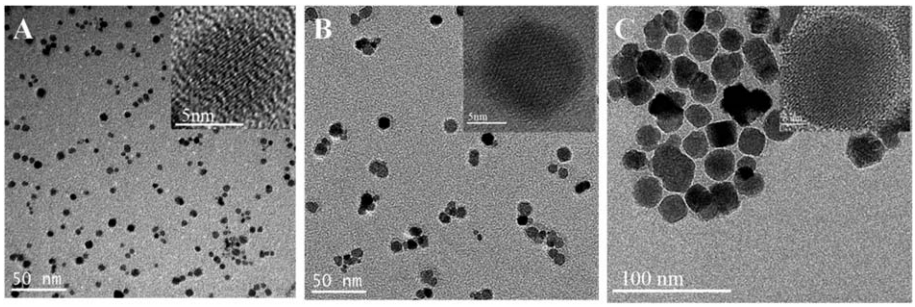

Fig. 1 TEM and HRTEM images (insets) of $BaTiO_3$ NPs with different diameters ((A) ~6 nm; (B) ~11 nm; (C) ~27 nm) using star-like PAA-*b*-PS diblock copolymers with different molecular weights as nanoreactors (sample-1, sample-2 and sample-3 in Table S1,† respectively).

miscibility of $BaTiO_3$ NPs within the host environment (*e.g.*, the polymer matrix as in polymer–NP nanocomposites), and thus further surface modification of NPs is not necessary. The existence of capped PS chains on the surface of $BaTiO_3$ NPs was confirmed by ^{1}H-NMR measurement. The PS-functionalized $BaTiO_3$NPs can be easily dissolved in toluene (Fig. S1†). The weight fractions of polymers in $BaTiO_3$-PS NPs were determined by TGA (Fig. S2†).

Fig. 2 shows the XRD patterns of PS-functionalized $BaTiO_3$NPs with different sizes (2θ = 43–47°; patterns with 2θ = 20–60° are shown in Fig. S3†). For the $BaTiO_3$ NPs with ~6 nm in diameter (sample-a), a single peak with 2θ at around 43–47° (corresponding to (200) lattice plane) was observed, suggesting the cubic phase of $BaTiO_3$ NPs. However, as the diameters increased to ~11 nm (sample-b) and ~27 nm (sample-c), the peak at 2θ around 43–47° split into two peaks. Detailed crystal structure refinement indicates that these $BaTiO_3$ NPs are largely tetragonal, with some detectable amounts of orthorhombic phase.[33] We note that theoretical and experimental studies[34–36] have been conducted on $BaTiO_3$ in order to identify the critical size, below which $BaTiO_3$ retains its cubic paraelectric structure at room temperature, yet there has still been no consensus on this issue.[36–39] Clearly, our results are in accordance with reports where the critical size of $BaTiO_3$ NPs was estimated to be on the order of 10–20 nm.[40] Moreover, the energy dispersive X-ray spectroscopy (EDS) microanalysis also substantiated the success in synthesizing PS-functionalized $BaTiO_3$ NPs (Fig. S4†).

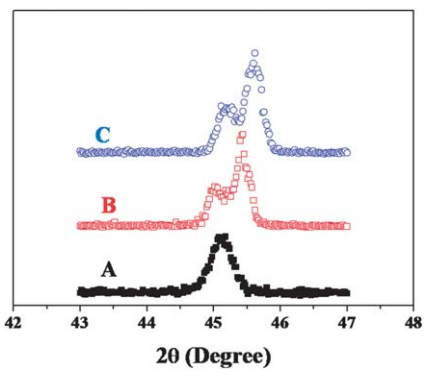

Fig. 2 XRD patterns of PS-functionalized $BaTiO_3$ NPs with different sizes. A (sample-a, D = ~6 nm), B (sample-b, D = ~11 nm), and C (sample-c, D = ~27 nm) are prepared by using different star-like PAA-*b*-PS block copolymers, *i.e.*, sample-1, sample-2, and sample-3 (Table S1†), respectively, as nanoreactors.

To prepare linear PS-*b*-PMMA diblock copolymer/PS-functionalized $BaTiO_3$ NP nanocomposites, two linear PS-*b*-PMMA diblock copolymers, in which PS blocks form the nanocylinders in the PMMA matrix (M_{PS} = 45 900 and M_{PMMA} = 138 000; and M_{PS} = 315 000 and M_{PMMA} = 785 000, respectively), were dissolved in toluene to make 5 mg mL^{-1} PS-*b*-PMMA toluene solution, in which PS-functionalized $BaTiO_3$ NP powder at different weight fractions of NP was added. Thin films of nanocomposites were prepared by spin-coating the toluene solution on the Si substrate and annealed under the saturated acetone vapor for a certain period of time at 25 °C. The key to using block copolymers to produce ordered block copolymer-based materials relies on the control over the orientation of nanodomains. The preferential interaction of the PMMA block with the Si substrate, together with the lower surface energy of the PS block in a cylinder-forming PS-*b*-PMMA diblock copolymer would favor orientation of cylindrical PS nanodomains parallel to the surface. To achieve closely packed arrays of PS nanocylinders oriented normal to the film surface in PS-*b*-PMMA as well as in PS-*b*-PMMA–PS-functionalized $BaTiO_3$ NP nanocomposites, selective solvent vapor annealing in a glass vessel was performed. Acetone was chosen as the selective solvent for the PMMA block as the polymer–solvent interaction parameter between PMMA and acetone $\chi_{PMMA/acetone}$ = 0.18 is much lower than that between PS and acetone $\chi_{PS/acetone}$ = 1.1.[41–43] The complete polymer–solvent miscibility can be realized at $\chi_{polymer-solvent} < 0.5$.[44]

The AFM and TEM images of pure PS-*b*-PMMA (M_{PS} = 45 900 and M_{PMMA} = 138 000) thin films before and after annealing with acetone vapor for 6.5 h (*i.e.*, without the addition of PS-functionalized $BaTiO_3$ NPs) are shown in Fig. 3. Compared to thin films before annealing where a featureless topology was observed (Fig. 3A and B), nearly hexagonally packed nanodomains were formed (Fig. 3C–F). This is not surprising as the saturated acetone vapor annealing process effectively enhanced the chain mobility for PS-*b*-PMMA by acting as a plasticizer. As a result, the PMMA matrix was swollen due to the absorption of acetone, and pulled from the PMMA/Si interface to contact preferentially with the acetone vapor (*i.e.*, air surface).[45] Since the PS domains can be selectively stained by ruthenium tetraoxide (RuO_4), the darker domains in the TEM images

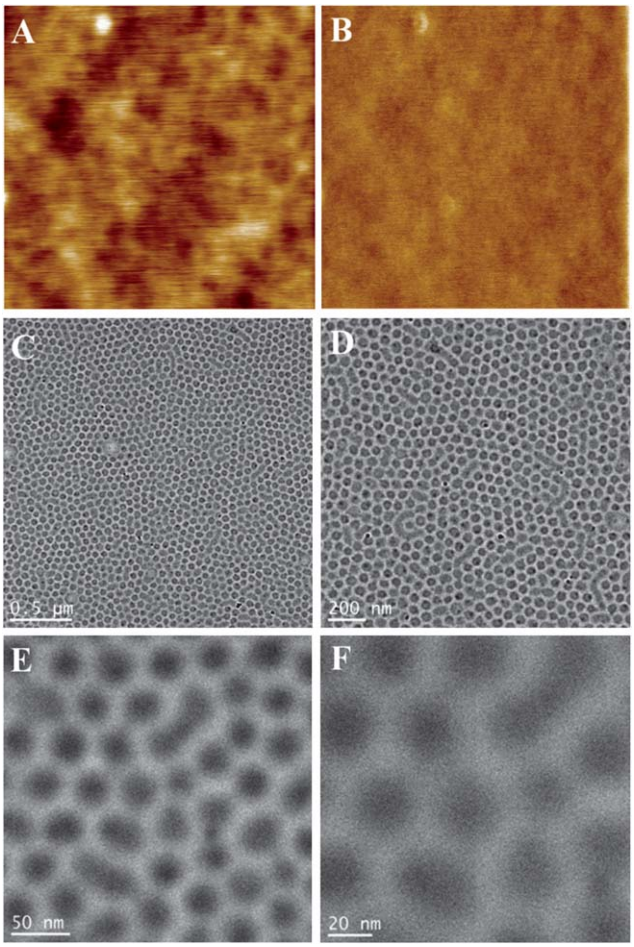

Fig. 3 AFM and TEM images of a pure PS-*b*-PMMA thin film (M_{PS} = 45 900 and M_{PMMA} = 138 000). (A) AFM height and (B) phase images of an as-prepared PS-*b*-PMMA thin film; image size = 5.0 × 5.0 μm^2, *Z* range = 6 nm for (A) and 3.3° for (B). (C–F) TEM images of a PS-*b*-PMMA thin film after exposing to the acetone vapor for 6.5 h. The closely packed arrays of PS nanodomains appeared dark in the bright PMMA matrix. The average diameter of PS nanocylinders is estimated to be 31.6 ± 3.8 nm, obtained by using standard image analysis software *ImageJ*. The film thickness was 42 nm.

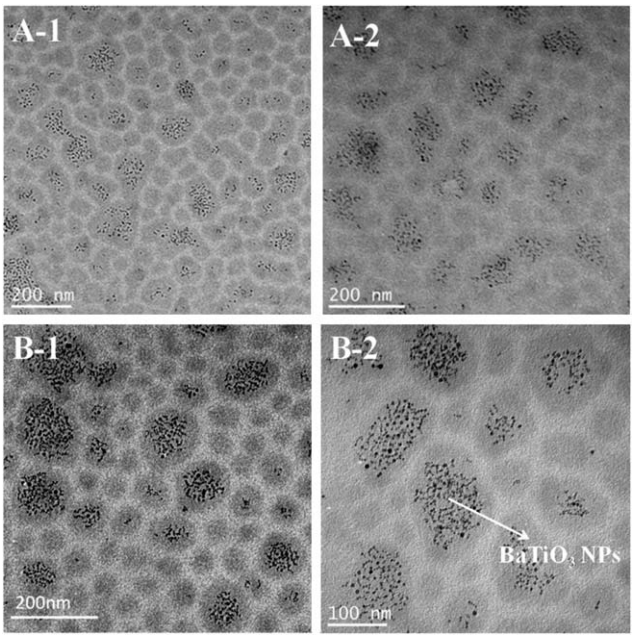

Fig. 4 TEM images of a thin film of PS-*b*-PMMA–PS-functionalized $BaTiO_3$ NP nanocomposite (sample-b, *D* = ~11 nm; M_{PS} = 45 900 and M_{PMMA} = 138 000) formed after the exposure to acetone vapor for 6.5 h. (A-1 and A-2) The volume fraction of $BaTiO_3$ NPs = 11.5%. (B-1 and B-2) The volume fraction of $BaTiO_3$ NPs = 16.3%. The closely packed cylindrical PS nanodomains containing $BaTiO_3$ NPs appeared dark. The average diameters of the PS nanocylinders after the addition of $BaTiO_3$ NPs are estimated to be 86.9 ± 20.4 nm (A-1 and A-2) and 112.5 ± 22.8 nm (B-1 and B-2), obtained by using standard image analysis software *ImageJ*. The film thickness was 52 nm in A-1 and A-2, and 55 nm in B-1 and B-2, respectively. The average numbers of $BaTiO_3$ NPs in the PS nanocylinders are approximately 54 (A-1 and A-2) and 76 (B-1 and B-2), respectively, calculated based on the volume fraction of $BaTiO_3$ NPs and the size of the PS nanocylinders.

correspond to the PS nanocylinders, while the PMMA matrix appears white.[46,47] The spacing between adjacent PS nanocylinders is approximately 46 nm.

Clearly, after the addition of PS-functionalized $BaTiO_3$ NPs (*e.g.*, sample-b) into PS-*b*-PMMA, the $BaTiO_3$ NPs were preferentially located in the PS nanocylinders (Fig. 4). This is a direct consequence of the surface capping of NPs with PS chains that is chemically identical to the PS block in PS-*b*-PMMA. Such permanent surface capping not only prevented $BaTiO_3$ NPs from aggregation by van der Waals forces, but also offered selective chemical affinity of $BaTiO_3$ NPs to the PS block against aggregation, *i.e.*, possessing a neutral χ_{NP-PS}, where χ_{NP-PS} represents the chemical affinity of the NP to the PS block (*i.e.*, enthalpic interaction). Interestingly, compared to some PS cylinders in Fig. 4 where no PS-functionalized $BaTiO_3$NPs were present, the existence of $BaTiO_3$ NPs enlarged cylindrical PS nanodomains due to the additions of surface-capped PS chains on the $BaTiO_3$ NPs to the PS nanodomains in PS-*b*-PMMA. Moreover, with the increased volume fraction of $BaTiO_3$ NPs, the size of PS nanodomains became larger (*e.g.*, comparing Fig. 4A-1 with Fig. 4B-1).

Similar to vertical PS nanocylinders formed in pure PS-*b*-PMMA upon annealing in the acetone vapor as discussed above (Fig. 3), the formation of vertically oriented PS nanocylinders containing $BaTiO_3$ NPs is illustrated in Scheme 1B, depicting the morphological reconstruction of the mixture of PS-*b*-PMMA–PS-functionalized $BaTiO_3$ NPs upon acetone vapor annealing. Such structural rearrangement was primarily due to the migration of the PMMA matrix, which interacted preferentially with acetone vapor. As PS and PMMA blocks are covalently linked at one end, the PS nanodomains rearranged themselves accordingly, thereby leading to a $BaTiO_3$ NP-containing nanocylinder normal to the surface of the nanocomposite film.[45] The weight loss and volume fractions of $BaTiO_3$ NPs in nanocomposites were determined by TGA (Fig. S5†). Based on the mass density of $BaTiO_3$ (6.02 g cm^{-3}), PS (1.05 g cm^{-3}) and PMMA (1.18 g cm^{-3}), the volume fractions of $BaTiO_3$ calculated from the mass loss in TGA tests were 11.5% and 16.3%, respectively (M_{PS} = 45 900 and M_{PMMA} = 138 000; *D* = ~11 nm) (Fig. S5†).

When asymmetric PS-*b*-PMMA with larger molecular weights of each block was used (*i.e.*, M_{PS} = 315 000 and M_{PMMA} = 785 000), closely packed nanodomains were also observed after the thin film was annealed in the acetone vapor for 6 h

(Fig. S6†). Likewise, the darker areas represented the PS nanodomains. The spacing between adjacent PS nanodomains is approximately 195 nm. After adding $BaTiO_3$ NPs of different sizes and volume fractions into PS-*b*-PMMA to form nanocomposites, it is clear that the $BaTiO_3$ NPs were localized within the PS nanodomains ($D = \sim 6$ nm and volume fraction = 10.8% in Fig. S7,† $D = \sim 6$ nm and volume fraction = 16.8% in Fig. S8† and $D = \sim 11$ nm and volume fraction = 15.9% Fig. S9†). Similarly, as the volume fraction of $BaTiO_3$ NPs increased, the size of PS nanodomains in the $BaTiO_3$ NP-loaded sample became larger than the unloaded sample.

The dielectric properties of PS-*b*-PMMA diblock copolymers and their corresponding nanocomposites in the frequency range of $f = 2$–15 GHz are shown in Fig. 5. The PS-*b*-PMMA diblock copolymers with relatively low molecular weight ($M_{PS} = 45\,900$ and $M_{PMMA} = 138\,000$) had a larger real part of permittivity ($\varepsilon' = 2.64 \pm 0.4$) than that of PS-*b*-PMMA with high molecular weight ($M_{PS} = 315\,000$ and $M_{PMMA} = 785\,000$) ($\varepsilon' = 2.45 \pm 0.2$) from $f = 2$–15 GHz. The decrease in ε' with an increase in molecular weight of diblock copolymers may be attributed to the higher degree of chain coiling for higher molecular weight polymers (*i.e.*, longer polymer chains) than for the low molecular weight polymers.[4] The nearly zero value of the imaginary part of permittivity ε'' indicates the dielectric lossless property of PS-*b*-PMMA diblock copolymers (Fig. 5A). The complex permittivity of the PS-*b*-PMMA ($M_{PS} = 45\,900$ and $M_{PMMA} = 138\,000$)/$BaTiO_3$ NP nanocomposites with the NP size of ~11 nm and ~27 nm is shown in Fig. 5B. For the nanocomposite loaded with ~27 nm $BaTiO_3$ NPs, the real part of permittivity, ε', was 21.11 ± 1.22, which is larger than that loaded with ~11 nm $BaTiO_3$ NPs ($\varepsilon' = 17.91 \pm 0.61$). This is likely due to the higher dielectric constant measured in the ~27 nm $BaTiO_3$ NPs compared with the ~11 nm $BaTiO_3$ NPs, *i.e.*, ~405 compared with ~260 measured at 1 MHz.[33] The imaginary part of permittivity, ε'', exhibited a steady value from $f = 2$–8 GHz, followed by an apparent increase from 8–15 GHz, indicative of the approach towards a resonance or relaxation at a frequency above the measured range, possibly a microstructural effect or a measurement artifact due to the microwave mode conversion caused by non-uniformities in the sample. The complex permittivity of nanocomposites prepared using the same series of $BaTiO_3$ NPs but PS-*b*-PMMA with higher molecular weight ($M_{PS} = 315\,000$ and $M_{PMMA} = 785\,000$) is shown in Fig. 5C. Both ε' and ε'' were found to be decreased when compared with the low molecular weight PS-*b*-PMMA ($M_{PS} = 45\,900$ and $M_{PMMA} = 138\,000$)/$BaTiO_3$ NP nanocomposites. The ε' of PS-*b*-PMMA ($M_{PS} = 315\,000$ and $M_{PMMA} = 785\,000$)/$BaTiO_3$ NP nanocomposites displayed a similar trend as the PS-*b*-PMMA ($M_{PS} = 45\,900$ and $M_{PMMA} = 138\,000$)/$BaTiO_3$ NP nanocomposites. The ε'' of two nanocomposites increased slightly over the entire frequency range, this may be because the resonant frequency of the resonant cavities is close to the higher end frequency (*i.e.*, 15 GHz). For the nanocomposites consisting of $BaTiO_3$ NPs of the same size but PS-*b*-PMMA with different molecular weights, the TGA results showed the nearly same volume fraction of NPs. Thus, the dielectric property difference between nanocomposites (*i.e.*, Fig. 5B and C) with the same

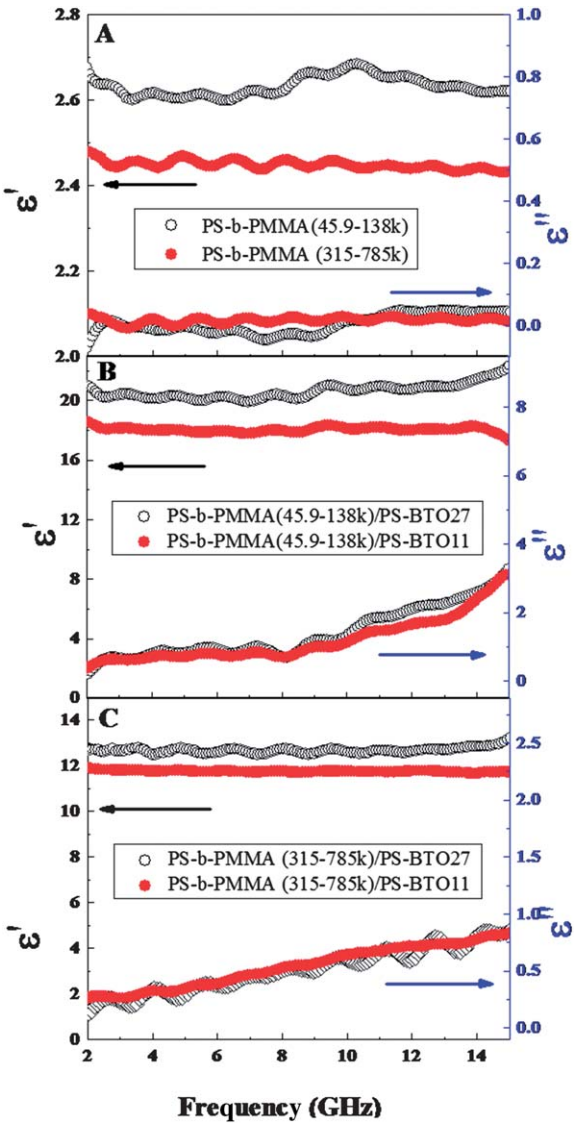

Fig. 5 The dielectric properties of pure PS-*b*-PMMA diblock copolymers and their corresponding nanocomposites in the microwave frequency range of 2–15 GHz. (A) Pure PS-*b*-PMMA without the addition of $BaTiO_3$ NPs. (B) PS-*b*-PMMA–PS-functionalized $BaTiO_3$ NP nanocomposites ($M_{PS} = 45\,900$ and $M_{PMMA} = 138\,000$) with the loading of different sized $BaTiO_3$ NPs (sample-b, $D = \sim 11$ nm, volume fraction of $BaTiO_3$ NPs = 11.5%; sample-c, $D = \sim 27$ nm, volume fraction of $BaTiO_3$ NPs = 11.2%). (C) PS-*b*-PMMA–PS-functionalized $BaTiO_3$ NP nanocomposites ($M_{PS} = 315\,000$ and $M_{PMMA} = 785\,000$) with the loading of different sized $BaTiO_3$ NPs (sample-b, $D = \sim 11$ nm, volume fraction of $BaTiO_3$ NPs = 11.7%; sample-c, $D = \sim 27$ nm, volume fraction of $BaTiO_3$ NPs = 10.3%).

sized $BaTiO_3$ NPs was due most likely to the PS-*b*-PMMA matrix of different molecular weights,[48] which displayed different dielectric properties as shown in Fig. 5A. On the other hand, due to the toroidal shape of samples needed for the dielectric measurements by a Vector Network Analyzer, the dielectric properties of PS in the microwave frequency range ($f = 2$–15 GHz) cannot be measured because of the brittle nature of PS and its low mechanical resistance. Therefore, the ε' of $BaTiO_3$ NPs in the GHz range with different sizes cannot be extracted from their nanocomposites. However, our previous study indicates that the ε' of the ~27 nm $BaTiO_3$ NPs in the MHz range is

significantly higher than that of the ~11 nm particles.[33] Thus, the difference in dielectric properties of nanocomposites with the same PS-*b*-PMMA matrix used can be attributed to the size effect of $BaTiO_3$ NPs.[33,49–51] Obviously, the results shown in Fig. 5 suggest that both the molecular weight of PS-*b*-PMMA as the matrix and the size of $BaTiO_3$ NPs as the inclusion have an effect on the resulting dielectric properties of PS-*b*-PMMA–PS-functionalized $BaTiO_3$ NP nanocomposites.

Conclusions

In summary, we demonstrated the formation of nanocomposites composed of linear cylinder-forming PS-*b*-PMMA diblock copolymers and PS-functionalized $BaTiO_3$ NPs in which the latter was selectively constrained within the PS block of PS-*b*-PMMA. Ferroelectric $BaTiO_3$ NPs with different sizes, permanently capped with PS chains, were first synthesized by capitalizing on amphiphilic unimolecular star-like PAA-*b*-PS block copolymers as a template. The linear PS-*b*-PMMA offered a matrix for controlling the spatial organization of $BaTiO_3$ NPs in nanocomposites. Vertically oriented PS nanocylinders containing PS-functionalized $BaTiO_3$ NPs were achieved by annealing the thin film of PS-*b*-PMMA/$BaTiO_3$ NP nanocomposites with acetone vapor. The resulting nanocomposites displayed a high dielectric constant in the microwave frequency range. The dielectric properties of ferroelectric nanocomposites were dependent on the molecular weight of PS-*b*-PMMA and the size of $BaTiO_3$ NPs. The use of star-like diblock copolymers as nanoreactors to yield functional NPs that are intimately and permanently connected with polymer chains on the surface may open an avenue to produce a large variety of NPs with superior chemical affinity to the target block in block copolymers. As such, by minimizing the enthalpic interaction between the block copolymer and NPs, block copolymer-based nanocomposites can be readily crafted, thereby facilitating the fundamental study of their structure–property relationships. Block copolymer/ferroelectric nanoparticle nanocomposites may find potential applications in capacitors, actuators, transducers, pyroelectric sensors, photorefractive materials, and optical modulators.

Acknowledgements

We gratefully acknowledge funding support from the Air Force Office of Scientific Research (FA9550-09-1-0388) and the National Science Foundation (CBET 1159048).

References

1 M. R. Bockstaller, R. A. Mickiewicz and E. L. Thomas, *Adv. Mater.*, 2005, **17**, 1331.
2 S.-S. Sun, C. Zhang, A. Ledbetter, S. Choi, K. Seo, C. E. Bonner, Jr, M. Drees and N. S. Sariciftci, *Appl. Phys. Lett.*, 2007, **90**, 043117.
3 M. R. Bockstaller, Y. Lapetnikov, S. Margel and E. L. Thomas, *J. Am. Chem. Soc.*, 2003, **125**, 5276.
4 L. Yang and N. Bowler, *IEEE Trans. Antennas Propag.*, 2012, **60**, 2727.
5 Y.-H. La, E. W. Edwards, S.-M. Park and P. F. Nealey, *Nano Lett.*, 2005, **5**, 1379.
6 Z. Ma, C. Cao, J. Yuan, Q. Liu and J. Wang, *Appl. Surf. Sci.*, 2012, **258**, 7556.
7 Y.-Q. Kang, M.-S. Cao, J. Yuan and X.-L. Shi, *Mater. Lett.*, 2009, **63**, 1344.
8 H.-A. Ho and M. Leclerc, *J. Am. Chem. Soc.*, 2004, **126**, 1384.
9 J. Lu, K.-S. Moon, J. Xu and C. P. Wong, *J. Mater. Chem.*, 2006, **16**, 1543.
10 S.-J. Jeon, S.-M. Yang, B. J. Kim, J. D. Petrie, S. G. Jang, E. J. Kramer, D. J. Pine and G.-R. Yi, *Chem. Mater.*, 2009, **21**, 3739.
11 J. J. Chiu, B. J. Kim, E. J. Kramer and D. J. Pine, *J. Am. Chem. Soc.*, 2005, **127**, 5036.
12 B. J. Kim, J. Bang, C. J. Hawker and E. J. Kramer, *Macromolecules*, 2006, **39**, 4108.
13 M. J. Misner, H. Skaff, T. Emrick and T. P. Russell, *Adv. Mater.*, 2003, **15**, 221.
14 B. Jaffe, W. R. Cook and H. Jaffe, *Piezoelectric ceramics*, Academic, London, 1971.
15 Y. Ma, E. Vileno, S. L. Suib and P. K. Dutta, *Chem. Mater.*, 1997, **9**, 3023.
16 I. Tsuyumoto, M. Kobayashi, T. Are and N. Yamazaki, *Chem. Mater.*, 2010, **22**, 3015.
17 K. J. Choi, M. Biegalski, Y. L. Li, A. Sharan, J. Schubert, R. Uecker, P. Reiche, Y. B. Chen, X. Q. Pan, V. Gopalan, L.-Q. Chen, D. G. Schlom and C. B. Eom, *Science*, 2004, **306**, 1005.
18 Z. Tian, X. Wang, L. Shu, T. Wang, T.-H. Song, Z. Gui and L. Li, *J. Am. Ceram. Soc.*, 2009, **92**, 830.
19 Q. Feng, M. Hirasawa, K. Kajiyoshi and K. Yanagisawa, *J. Am. Ceram. Soc.*, 2005, **88**, 1415.
20 E.-W. Shi, C.-T. Xia, W.-Z. Zhong, B.-G. Wang and C.-D. Feng, *J. Am. Ceram. Soc.*, 1997, **80**, 1567.
21 E. B. Slamovich and I. A. Aksay, *J. Am. Ceram. Soc.*, 1996, **79**, 239.
22 H. Shimooka and M. Kuwabara, *J. Am. Ceram. Soc.*, 1996, **79**, 2983.
23 M. H. Frey and D. A. Payne, *Chem. Mater.*, 1995, **7**, 123.
24 W.-S. Cho, *J. Phys. Chem. Solids*, 1998, **59**, 659.
25 H.-I. Hsiang and F.-S. Yen, *J. Am. Ceram. Soc.*, 1996, **79**, 1053.
26 X. Pang, L. Zhao, M. Akinc, J. K. Kim and Z. Lin, *Macromolecules*, 2011, **44**, 3746.
27 A. M. Nicholson and G. F. Ross, *IEEE Trans. Instrum. Meas.*, 1970, **IM-19**, 377.
28 W. B. Weir, *Proc. IEEE*, 1974, **62**, 33.
29 S. W. Lu, B. I. Lee, Z. L. Wang and W. D. Samuels, *J. Cryst. Growth*, 2000, **219**, 269.
30 M. H. Frey and D. A. Payne, *Phys. Rev. B: Condens. Matter Mater. Phys.*, 1996, **54**, 3158.
31 K. Matyjaszewski, S. G. Gaynor, A. Kulfan and M. Podwika, *Macromolecules*, 1997, **30**, 5192.
32 N. V. Tsarevsky and K. Matyjaszewski, *Chem. Rev.*, 2007, **107**, 2270.
33 H. Z. Guo, Y. Mudryk, M. I. Ahmad, X. C. Pang, L. Zhao, M. Akinc, V. K. Pecharsky, N. Bowler, Z. Q. Lin and X. Tan, *J. Mater. Chem.*, 2012, **22**, 23944.

34 Y. Fukui, S. Izumisawa, T. Atake, A. Hamano, T. Shirakami and H. Ikawa, *Ferroelectrics*, 1997, **203**, 227.
35 A. V. Polotai, A. V. Ragulya and C. A. Randall, *Ferroelectrics*, 2003, **288**, 93.
36 T. Hoshina, H. Kakemoto, T. Tsurumi, S. Wada and M. Yashima, *J. Appl. Phys.*, 2006, **99**, 054311.
37 K. Uchino, E. Sadanaga and T. Hirose, *J. Am. Ceram. Soc.*, 1989, **72**, 1555.
38 S. Aoyagi, Y. Kuroiwa, A. Sawada, I. Yamashita and T. Atake, *J. Phys. Soc. Jpn.*, 2002, **71**, 1218.
39 Y. G. Wang, W. L. Zhong and P. L. Zhang, *Solid State Commun.*, 1994, **90**, 329.
40 D. McCauley, R. E. Newnham and C. A. Randall, *J. Am. Ceram. Soc.*, 1998, **81**, 979.
41 Y. Xuan, J. Peng, L. Cui, H. Wang, B. Li and Y. Han, *Macromolecules*, 2004, **37**, 7301.
42 Y. Chen, H. Huang, Z. Hu and T. He, *Langmuir*, 2004, **20**, 3805.
43 J. Peng, D. H. Kim, W. Knoll, Y. Xuan, B. Li and Y. Han, *J. Chem. Phys.*, 2006, **125**, 064702.
44 Y. Xuan, J. Peng, L. Cui, H. Wang, B. Li and Y. Han, *Macromolecules*, 2004, **37**, 7301.
45 S. W. Hong, J. Wang and Z. Lin, *Angew. Chem., Int. Ed.*, 2009, **48**, 8356.
46 Y. Chen, H. Huang, Z. Hu and T. He, *Langmuir*, 2004, **20**, 3805.
47 U. Jeong, H. C. Kim, R. L. Rodriguez, I. Y. Tsai, C. M. Stafford, J. K. Kim, C. J. Hawker and T. P. Russell, *Adv. Mater.*, 2002, **14**, 274.
48 J. M. Garnett, *Philos. Trans. R. Soc., A*, 1906, 237.
49 J. E. Spanier, A. M. Kolpak, J. J. Urban, I. Grinberg, L. Ouyang, W. S. Yun, A. M. Rappe and H. Park, *Nano Lett.*, 2006, **6**, 735.
50 C. L. Wang and S. R. P. Smith, *J. Phys.: Condens. Matter*, 1995, 7163.
51 J. J. Urban, J. E. Spanier, L. Ouyang, W. S. Yun and H. Park, *Adv. Mater.*, 2003, **15**, 423.

